PRODUCTION MANAGEMENT

Improving the wear resistance of copper tools for pressure die casting by laser melt injection

Philipp Warneke[1] · Annika Bohlen[1] · Thomas Seefeld[1]

Abstract

Highly conductive copper alloys are used for various tools in casting and welding technology. In pressure die casting, copper alloys are used for pistons pressing the metal melt into a die. The high thermal conductivity of these alloys allows short process times as a result of high cooling rates. Due to a poor wear resistance, wear occurs on the running surface of the pistons causing the metal melt to spurt out of the shot sleeve. In order to improve the service life of the pistons, a new approach was taken: a reinforcement of the copper alloys with fused tungsten carbide (FTC) particles by laser melt injection (LMI) at high process velocities. FTC provides a hardness between 2700 HV 0.1 and 3500 HV 0.1. During LMI, a melt pool is induced on the substrate by a laser beam and a filler material is injected into this melt pool by a powder nozzle. In contrast to laser cladding, the filler material remains in the solid state and the substrate works as matrix material. Thereby, specific material properties of the substrate—e.g. a high thermal conductivity—can be preserved within the surface layer. It was shown that the FTC particle reinforcement reduced the wear by 69–75%. Abrasion and adhesion were identified as the dominant wear mechanisms. The run-in behavior of FTC particle reinforced and non-reinforced parts was determined.

Keywords Laser melt injection · Metal-matrix composite · Wear protection · Sliding wear · Pressure die casting

1 Introduction

In pressure die casting, a piston presses molten metal into a die at press velocities up to 7 m/s and pressures up to 800 MPa, see Fig. 1 [1]. This is a widely spread casting technology for the large-scale production of parts made of non-ferrous metals such as aluminum and zinc alloys [2]. Due to a good ability for automation, a fast filling of the die and high cooling rates, pressure die casting is the most productive technology for producing cast parts [1]. The high cooling rates and corresponding short process cycles can be achieved by pistons made of highly conductive copper alloys. However, the limited wear resistance of the copper alloys causes high manufacturing costs. In order to improve

the wear resistance, a reinforcement of the copper alloys by hard particles is intended. Accordingly, a metal matrix composite (MMC) layer is generated on the surface of the pistons.

In previous research, various techniques for generating copper alloy matrix composites were investigated. Sintering is a very common technique for generating MMCs that was also used for copper substrates [3, 4]. Besides, an infrared infiltration technique [5] and friction stir processing [6] were investigated for reinforcing copper with hard particles. For infrared filtration, a tungsten carbide preform and a copper block are placed in a graphite crucible and heated up over the melting point of copper by infrared radiation. During friction stir processing, silicon carbide particles are compressed into a groove of a copper plate before they are dispersed into the copper plate by friction stir welding. All three techniques, however, require extensive preparations making an industrial application difficult. In contrast, laser melt injection (LMI) allows one step processing on various workpiece geometries.

LMI is a process for generating wear-resistant MMC layers on metallic substrates that first came up in the 1980s [7]. The principle of LMI for rotationally symmetrical parts is shown in Fig. 2. Steel [8], aluminum alloys [9],

✉ Philipp Warneke
warneke@bias.de

Annika Bohlen
bohlen@bias.de

Thomas Seefeld
seefeld@bias.de

1 BIAS-Bremer Institut für Angewandte Strahltechnik GmbH, Klagenfurter Straße 5, 28359 Bremen, Germany
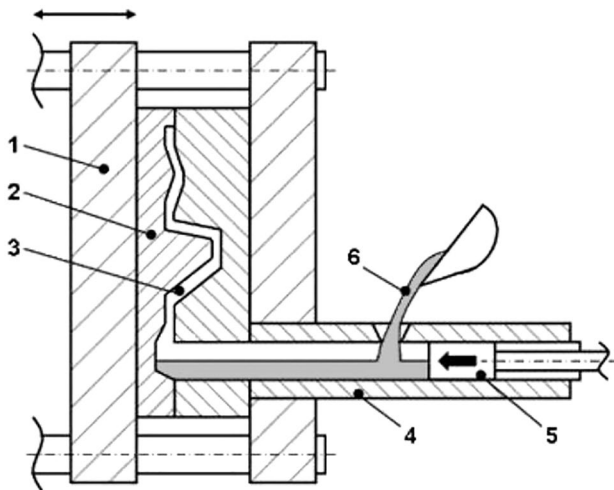
Fig. 1 Principle of cold chamber pressure die casting [1]. A piston (5), that runs in a shot sleeve (4), presses the melt (6) into the cavity (3) of a die (2). The die (2) is supported by a frame (1)
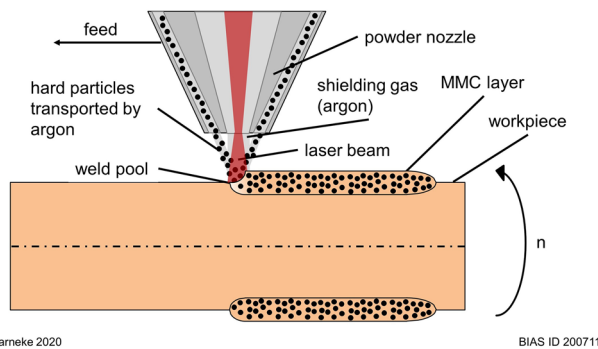

Fig. 2 Principle of LMI for rotationally symmetrical parts. A laser beam generates a weld pool on a workpiece. Hard particles are injected into the weld pool by a powder nozzle

aluminum bronze [10] and titanium alloys [11] were investigated as substrate materials. As hard materials, largely metallic hard materials, such as tungsten carbide, were used. Silicon carbide is a very common hard material for reinforcing aluminum alloys. For reinforcing copper alloys, fused tungsten carbide (FTC) is selected due to its combination of a high hardness and a high fracture toughness [12]. Furthermore, tungsten carbide features a superior wetting behavior in a metallic melt [13].

The low absorption of only 5% of infrared laser light by solid copper (smooth surface, perpendicular incidence) [14] makes laser processing very difficult. In a previous work, nevertheless, it was shown that homogeneous MMC layers can be generated on the copper alloy Hovadur® CNCS with the help of high laser intensities of up to 191 kW/cm² and a tilt of the processing optic of 20° [15].

For measuring the improvement in wear resistance by the hard particle reinforcement, oscillating wear tests on hard particle reinforced and non-reinforced samples with a pin on cylinder setup were carried out in a tribometer. Similar tests were performed on hard particle reinforced copper samples by Tjong and Lau [4] and by Deshpande and Lin [16]. A rotating silicon carbide disc was used as counter body (pin on disc test). Tjong and Lau investigated the wear volume at different contents of titanium diboride particles between 0 and 20 vol%. It was determined that the wear volume decreases with an increasing content of titanium diboride particles. After a sliding distance of 100 m at a test force of 15 N, the wear volume of the sample with 20 vol% titanium diboride was only 0.5% of the wear volume of the non-reinforced sample. Deshpande and Lin stated that the wear rate of non-reinforced copper increases significantly with an increasing test force. In contrast, the increase of the wear rate of a copper sample reinforced by 53 vol% tungsten carbide is comparatively low. The wear rate of reinforced copper is 5% of the wear rate of non-reinforced copper after a sliding distance of 500 m at a test force of 4 N.

To sum up, copper matrix composites are a promising material for applications where a high thermal or electrical conductivity as well as a high wear resistance are needed. In previous research, it could be shown that the reinforcement of copper by metallic hard materials such as titanium diboride or tungsten carbide leads to a significant improvement in wear resistance. In this work, investigations on the wear behavior of FTC reinforced copper matrix composites that were generated by LMI are presented and discussed. In contrast to other manufacturing processes for copper matrix composites, LMI allows one step processing and local machining.

2 Materials and methods

2.1 Materials

Table 1 gives an overview about the used materials. The substrate is made of Hovadur® CNCS, a precipitation hardened copper alloy featuring a high thermal conductivity of 220 W/mK. Cylindrical workpieces made of this material were turned to a diameter of 80 mm. FTC particles with a spherical shape (Oerlikon MetcoClad 52001) and a grain fraction between 45 and 106 μm were injected into the Hovadur® CNCS substrate by LMI. FTC is an eutectic material of 20…27% WC and 73…80% W_2C [13]. The FTC particles in the initial state are shown in Fig. 3. The particle size of the FTC particles is homogeneously distributed, see Table 2. The steel 1.2343 was selected as material for the counter bodies in the wear tests because it is a common alloy for shot sleeves in pressure die casting. The counter bodies

Table 1 Materials used for LMI and tribological experiments

Material	Hovadur® CNCS	FTC	1.2343
Chemical composition in wt%	Ni: 2…3 Si: 0.5…0.8 Cr: 0.2…0.5 Fe: max. 0.15 Mn: max. 0.1 Pb: max. 0.02 others: max. 0.1 Cu: balance [17]	C: 3.8 Others: 0.7 W: balance [18]	C: 0.38 Si: 1.1 Mn: 0.4 Cr: 5.0 Mo: 1.3 V: 0.4 Fe: balance [19]
Density in g/cm^3	8.8 [17]	16 [20]	7.8 [19]
Hardness	190 HB [17]	2700…3500 HV 0.1 [18]	1100…1200 HV 1 after hardening and gas nitriding
Thermal conductivity in W/(m · K)	220 [17]	n/a	25 [19]
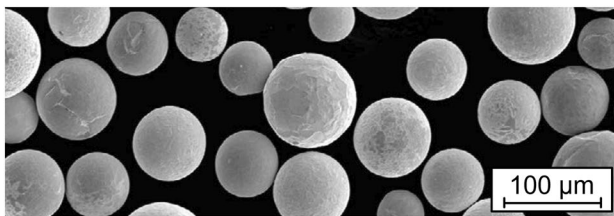
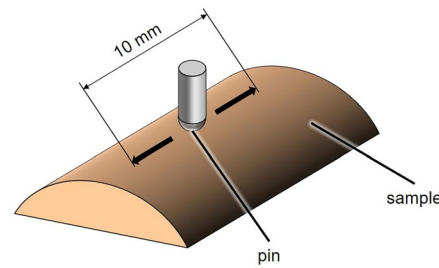**Fig. 3** SEM image of spherical FTC powder particles (Oerlikon MetcoClad 52001) [18]

Table 2 FTC particle size distribution

Particle size in μm	Proportion in wt%
< 45	3.9
45…75	47.9
75…106	47.0
> 106	1.3

Fig. 4 Schematic of an oscillating wear test on a cylindrical sample surface. The pin moves sinusoidally on the sample

featured a cylindrical shape with a diameter of 10 mm and a spherical cap with a radius of 5 mm. They were vacuum hardened in three steps at 1040 °C and tempered two times. Afterwards, the counter bodies were gas nitrided for 6.5 h.

2.2 Laser melt injection

A disc laser (Trumpf TruDisk 12,002) emitted radiation with a wavelength of 1030 nm that was guided to a processing optic (Trumpf BEO D70) by an optical fiber with a diameter of 200 μm. The collimating lens of the processing optic provided a focal length of 200 mm, whereas the focusing lens provided a focal length of 300 mm. The processing optic was carried by a six-axis robot (Reis) that moved the processing optic parallel to the rotational axis of the workpiece. In order to avoid any damages caused by reflections, the focusing optic was tilted by 20° from the vertical in direction of travel. The workpiece was positioned 15 mm below the laser focus obtaining a laser spot with a diameter of 2 mm. A three-jet powder nozzle (IXUN) was used with a working distance of 16 mm. The FTC particles were transported to the powder nozzle by a powder feeder (GTV PF 2/2). Argon was used as feeding gas with a flow rate of 15 l/min and as shielding gas with a flow rate of 8 l/min. The lateral trace offset was set to 1 mm. LMI with a laser power of 4 kW and a process speed of 5 m/min was carried out on cylindrical workpieces made of Hovadur® CNCS with a diameter of 80 mm.

2.3 Tribological testing and analysis

After LMI, the workpieces were machined by cylindrical grinding. A non-reinforced Hovadur® CNCS workpiece with a diameter of 80 mm and a turned surface was used for preparing non-reinforced samples. The samples were cut out of the cylindrical parts by EDM. Figure 4 shows the schematic set-up for the wear tests. For conducting the wear tests, a tribometer (CETR UMT 3) was used. The tribometer was placed inside a box in which the

temperature and the humidity could be controlled. The temperature was kept at 25 °C ± 0.1 °C and the humidity between 50 and 55%. For all tests, the frequency for the oscillating movement was 5 Hz and the distance between the turning points was 10 mm, see Fig. 4, leading to an average test speed of 100 mm/s. Test forces of 15 and 30 N were applied over a test time of 4 h. For each test force and FTC particle content, three tests were conducted. In contrast, the tests for the run-in behavior were conducted once. For determining the run-in behavior, wear tests with a non-reinforced sample and an FTC particle reinforced Hovadur® CNCS sample featuring a particle content of 40 vol% were carried out. At a test force of 30 N, tests with each sample were carried out for twelve periods of 30 min. After each period, the wear height and the wear volume were determined.

The wear height on the samples and the pins was determined geometrically according to DIN EN 1071-12 [21]. In contrast to DIN EN 1071-12, the surfaces were not flat but cylindrical (sample) and spherical (pin). Depending on whether the wear profile was convex-shaped or concave-shaped, the wear height h_w was calculated from the height of circular segment h_1 and the measured height h_2 according to Fig. 5. A confocal microscope (Keyence VK9700) and the software VK Analyzer were used for determining the width of the wear tracks s and the height h_2 at six positions for each sample and pin. The z-resolution during

confocal microscopy was 2 μm. The height of circular segment h_1 is given by

$$h_1 = r - \sqrt{r^2 - \frac{1}{4}s^2} \tag{1}$$

Since the radius r and the width of the wear track s are known. The radius r is given by the geometry of the workpiece.

For determining the wear volume, the weight loss of the samples and the pins was measured with a high-precision scale (Shimadzu AUW120D, reading accuracy $d = 0.1$ mg). The calculation of the wear volumes was based on combined densities considering the FTC particle content.

2.4 Metallographic analysis

The MMC specimens were cut by an Agiecut Evolution 2 eroding machine and hot mounted into Struers LevoFast. After grinding the mounted specimens with a granulation from P320 to P1200, they were polished by a diamond suspension featuring a particle size of 3 μm and by a silicon oxide suspension featuring a particle size of 0.04 μm. Micrographs were taken with a Zeiss AX10. Furthermore, a Struers DuraScan 50 was used for measuring the Vickers hardness of the hard particles and the Hovadur® CNCS matrix with a test force of 0.1 kP. For measuring the overall hardness of the MMC layer, a test force of 10 kP was
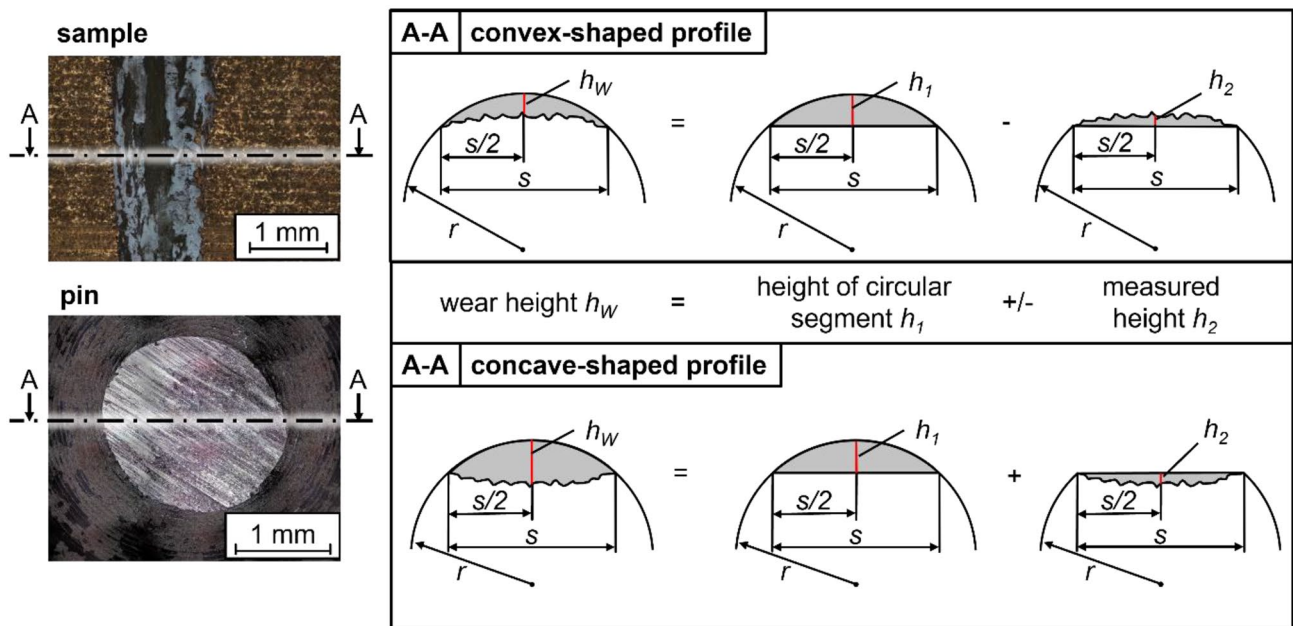
Fig. 5 Method for geometrical measurement of the wear height of sample and pin. The width of the wear track s and the height h_2 were measured with the software VK Analyzer
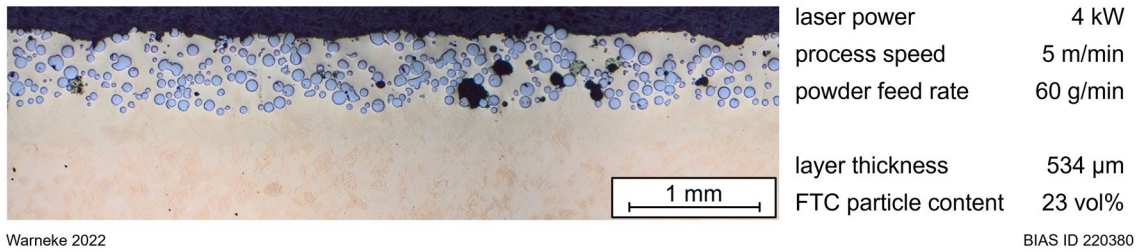
laser power	4 kW
process speed	5 m/min
powder feed rate	60 g/min
layer thickness	534 µm
FTC particle content	23 vol%

Warneke 2022   BIAS ID 220380

Fig. 6 Cross section of an MMC layer generated by LMI on Hovadur® CNCS

Warneke 2022   BIAS ID 220381
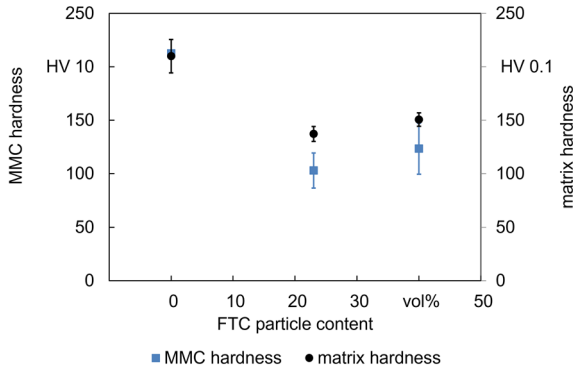
Fig. 7 Overall hardness of the MMC layer and hardness of the Hovadur® CNCS matrix

Warneke 2022   BIAS ID 220382

Fig. 8 Hardness of the FTC particles after LMI

applied for creating indentations that cover several FTC particles. For measuring the layer thickness and the FTC particle content, the software ImageJ was used. The layer thickness was measured on a cross section. The FTC particle content was measured by area on a micrograph taken from the surface of a sample as described in 2.3. The FTC particle area was encircled manually on the image within a ROI and the percentage of the FTC particle area was determined accordingly.

3 Results and discussion

With LMI, homogenous MMC layers can be generated on Hovadur® CNCS. Figure 6 shows a cross section of FTC particle reinforced Hovadur® CNCS directly after LMI. The hardness of the Hovadur® CNCS matrix decreases by LMI since the precipitations are dissolved when melting the substrate with the laser beam, see Fig. 7. Furthermore, the overall hardness of the MMC layer (matrix and FTC particles) decreases by LMI. It can be assumed that the indenter presses the FTC particles into the soft Hovadur® CNCS matrix during hardness testing. However, the hardness of the FTC particles is not affected by the LMI process. The
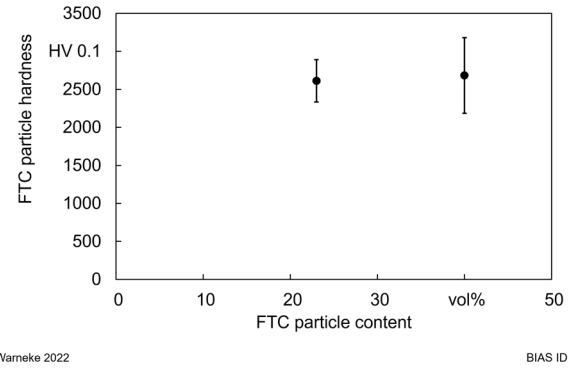

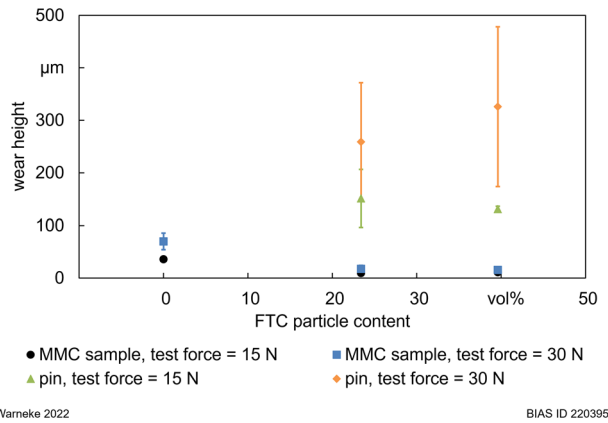Warneke 2022   BIAS ID 220395

Fig. 9 Geometrical analysis: wear height of non-reinforced and FTC particle reinforced Hovadur® CNCS samples and the corresponding pins. Test time = 4 h. The standard deviation was calculated from three test results for each test force and FTC particle content

hardness after LMI is within the range of the initial hardness (2700…3500 HV 0.1), see Fig. 8.

The wear height is the most important wear measuring quantity for pistons in pressure die casting. The wear height of non-reinforced and FTC particle reinforced Hovadur® CNCS samples featuring a particle content of 23 and 40 vol% was measured in order to determine the improvement in wear resistance through the FTC particle

reinforcement. Figure 9 shows that the FTC particle reinforcement improves the wear resistance significantly. The wear height is reduced by 69% at a test force of 15 N and by 75% at a test force of 30 N. It is notable that the wear resistance does not further increase with a higher FTC particle content. In contrast, the wear height of the pin increases drastically by the FTC reinforcement of Hovadur® CNCS. Whereas no wear can be detected on the pins that ran on non-reinforced Hovadur® CNCS, strong wear occurs when the pins run on FTC particle reinforced Hovadur® CNCS.

In other works about the wear resistance of MMCs, it was found that the wear resistance increases with the particle content. In titanium diboride reinforced copper, the wear volume decreases from 0.6 to 0.1 mm^3 after a sliding distance of 100 m at a test force of 15 N when the titanium diboride particle content is increased from 10 to 20 vol%.
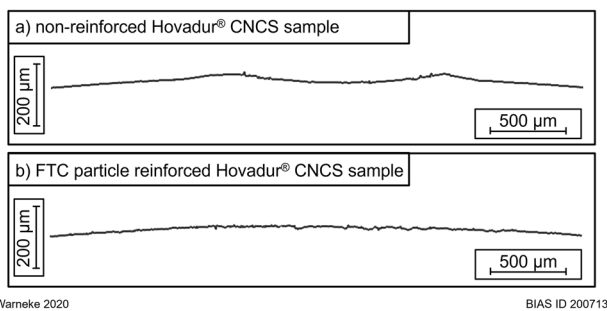
Fig. 10 Profiles perpendicular to test movement obtained by confocal microscopy. Test force = 15 N, test time = 4 h, FTC particle content = 40 vol%

[4]. A similar behavior was observed for tungsten carbide reinforced tool steel [22] and an aluminum oxide reinforced aluminum alloy [23]. However, it was also found that the dependence of the wear resistance on the particle content is strongly affected by the material combination of matrix and particle [24]. FTC particle reinforced Hovadur® CNCS contains extremely hard particles in a soft matrix. Furthermore, the FTC particles are significantly harder than the pins. Consequently, mainly the pin wears out when Hovadur® CNCS is reinforced by FTC particles.

The wear behaviour of the non-reinforced Hovadur® CNCS sample clearly differs from the wear behavior of the FTC particle reinforced sample. The wear areas showed different geometries. The non-reinforced wear areas showed a concave profile because the counter body did not wear out, see Fig. 10a. The wear track is less wide but deeper than the wear track of an FTC particle reinforced Hovadur® CNCS sample. In contrast, a convex geometry was observed on the reinforced wear area since the counter body showed significant wear, see Fig. 10b.

The steel pins out of hardened and gas nitrided 1.2343 provide a strong wear resistance. The comparatively soft Hovadur® CNCS wears out heavily when being in touch with the steel pin. The steel pin does not wear out and the pin intrudes into the Hovadur® CNCS sample. No wear could be determined on the steel pins at a test force of 15 and 30 N. However, Fig. 11a shows slight deformations on the surface of the pin that was in touch with the Hovadur® CNCS sample. In contrast, when moving on an FTC particle reinforced sample, the steel pin wears out heavily. Because of the initial spherical geometry of the
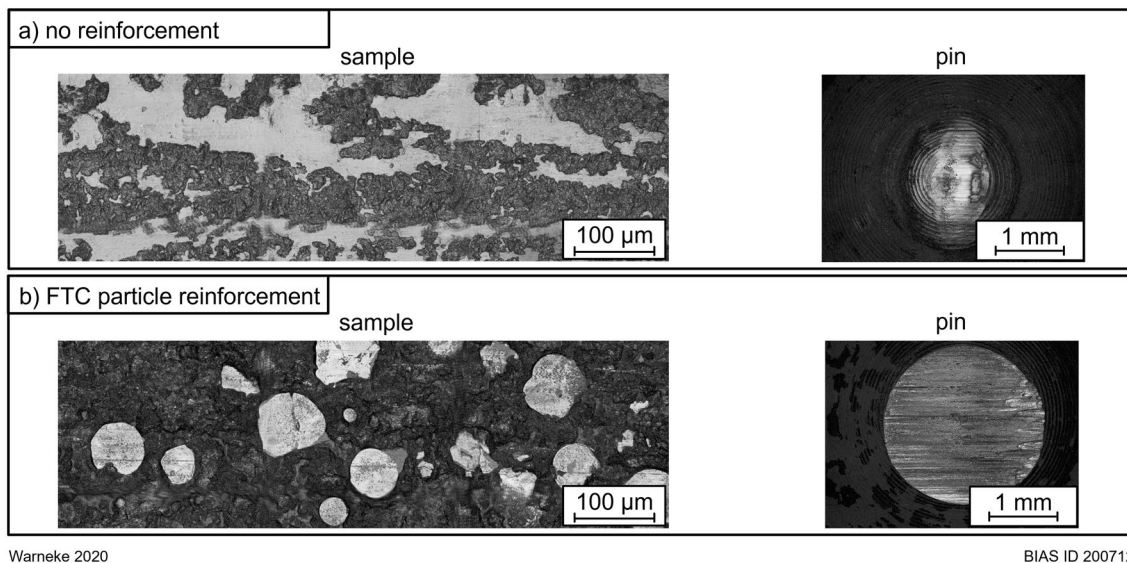

Fig. 11 Laser microscope images: wear tracks of a non-reinforced (**a**) and an FTC particle reinforced (**b**) Hovadur® CNCS sample and the corresponding pins. The spherical shaped FTC particles are clearly identifiable on the FTC particle reinforced sample (**b**). Test force = 30 N, test time = 4 h, FTC particle content = 40 vol%

steel pin, the contact area between sample and pin grows significantly resulting in a large width of the wear tracks on the Hovadur® CNCS sample and on the pin.

For analyzing the wear mechanisms, confocal microscope images and EDX mappings were investigated. Figures 11 and 12 show the same region of the wear tracks of the samples and the pins. Both on the non-reinforced wear track and on the FTC particle reinforced wear track of the samples, two different areas can be identified. Whereas the one area features a smooth topography (light gray in Fig. 11), the other one is characterized by a rugged topography (dark gray in Fig. 11). On the FTC particle reinforced wear track, the FTC particles represent the smooth area and are surrounded by a rugged matrix. The FTC particles protrude up to 15 µm from the matrix, see Fig. 12b. In contrast, the smooth area on the non-reinforced wear track is only a few micrometers higher than the rugged area, see Fig. 12a. In a previous work, by carrying out EDX mappings on the wear tracks, it was shown that no significant transfer of material from the sample to the pin or the other way round could be found neither on the non-reinforced and the FTC particle reinforced Hovadur® CNCS sample [25]. Figure 13 shows the EDX mappings of a non-reinforced and an FTC particle reinforced Hovadur® CNCS sample. On the non-reinforced wear track, mainly copper was detected, whereas the FTC particles can be identified by tungsten rich areas on the FTC particle reinforced wear track. Furthermore, small iron rich areas were detected which may represent abrasive particles from the steel pin that are attached onto the wear track's surface.

The occurrence of wear mechanisms depends on the tribological system. The combination of materials, the use of lubricants and the temperature are part of this system. Furthermore, the tribological stress on the sample and the counter body is an important factor. Copper and bronze alloys are known for adhesion wear. In deep drawing, for example, adhesion wear occurs on FTC particle reinforced bronze tools in addition to abrasion wear [26]. On the non-reinforced and the FTC particle reinforced Hovadur® CNCS sample, both abrasion wear and adhesion wear can be found as well. Although no significant transfer of material is indicated by the EDX mapping results, the rugged areas on the wear tracks of the samples are a clear indication for adhesion wear. On the FTC particle reinforced Hovadur® CNCS sample, a high wear resistance of the FTC particles leads to a significant height difference between the FTC particles and the Hovadur® CNCS matrix. Since abrasive particles that were formed during the wear tests were not removed during the tests, it is also possible that some of these particles were attached to the sample's surface as a consequence of high pressure. This would affect the topography, too.

In the following, the run-in behavior of a non-reinforced, of an FTC particle reinforced Hovadur® CNCS sample and of the corresponding counter bodies is presented. The wear-time diagrams of the Hovadur® CNCS samples are shown in Figs. 14 and 15. The wear height measurements show a high standard deviation, see Fig. 14. Overall, the wear height increases with time on the non-reinforced Hovadur® CNCS sample as well as on the FTC particle reinforced Hovadur® CNCS sample. But the values scatter heavily. One reason for the strong scattering of the wear height of the Hovadur®
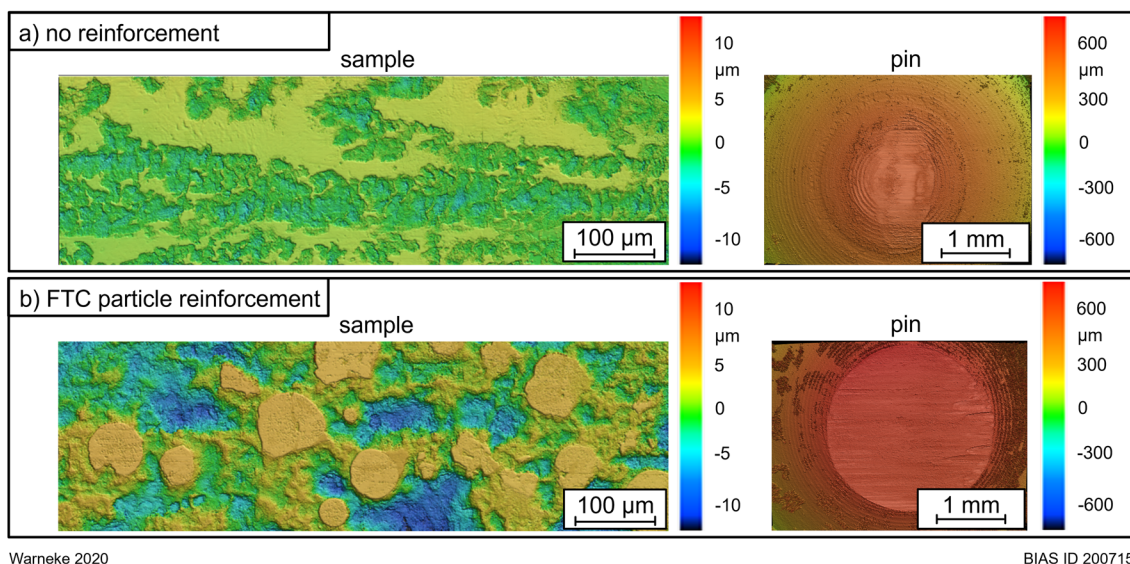

Fig. 12 3D scans: wear tracks of a non-reinforced (**a**) and an FTC particle reinforced (**b**) Hovadur® CNCS sample and the corresponding pins. Test force = 30 N, test time = 4 h, FTC particle content = 40 vol%
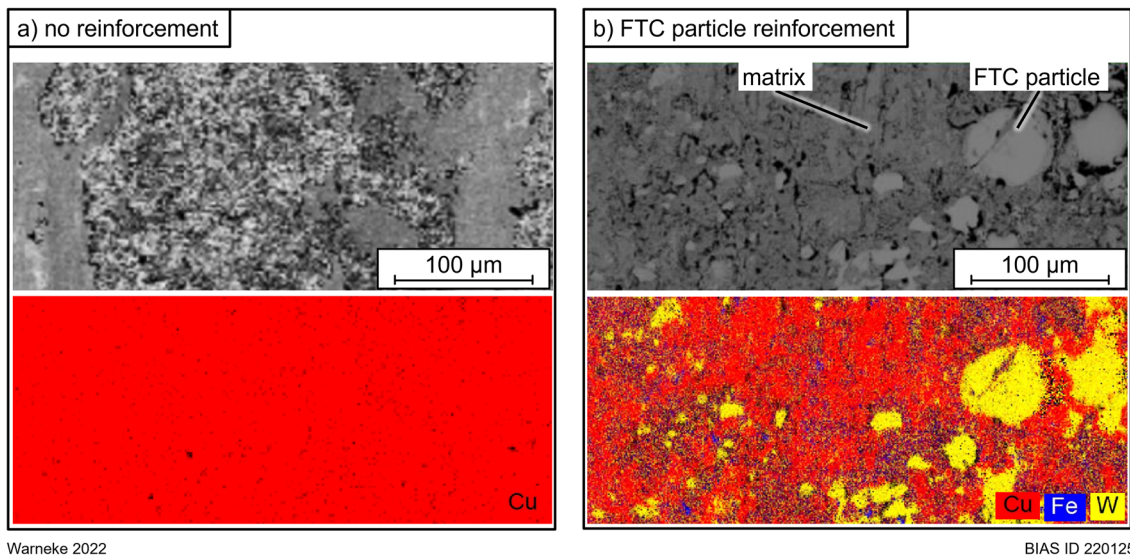
Fig. 13 SEM images (top) and EDX mappings (bottom) of a non-reinforced (**a**) and an FTC particle reinforced (**b**) Hovadur® CNCS sample. Test force = 30 N, test time = 4 h, FTC particle content = 40 vol%
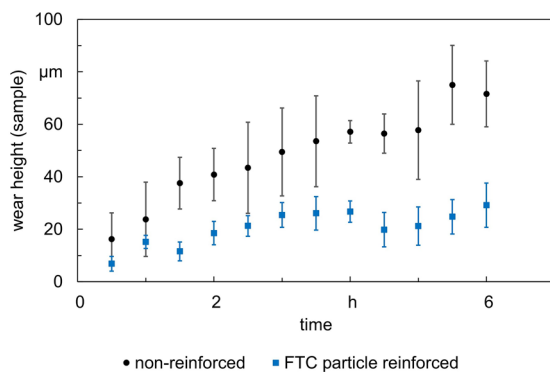

Fig. 14 Geometrical analysis: run-in behavior of a non-reinforced and an FTC particle reinforced Hovadur® CNCS sample. Test force = 30 N, FTC particle content = 40 vol%. The standard deviation is based on six measurements of the wear height
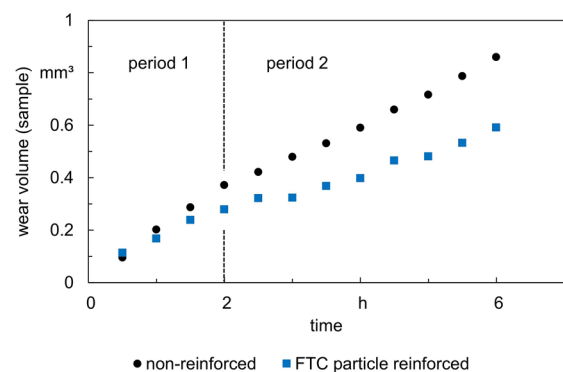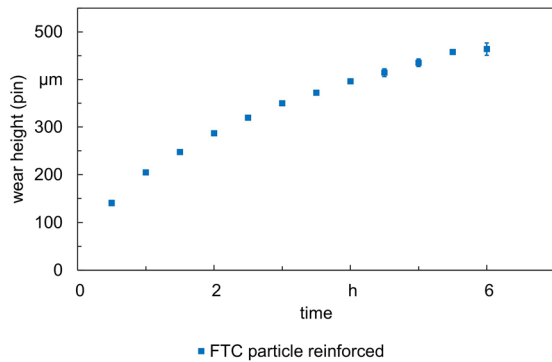
Fig. 15 Gravimetrical analysis: run-in behavior of a non-reinforced and an FTC particle reinforced Hovadur® CNCS sample. Test force = 30 N, FTC particle content = 40 vol%. The standard deviation is based on three weight measurements and is too small for being identifiable in the diagram

CNCS samples are differences in the width and the height along the wear track. The position of the measuring points has a clear influence on the result even though the average is calculated from six single measurements.

In contrast, the gravimetrical results scatter less. Here, the standard deviation of the measurements is negligible. The wear volume progression could be divided into two different periods, see Fig. 15. Period one extended from the beginning of the experiment to a test time of two hours. During this period, a degressive increase of the wear volume could be observed for both samples even though the increase of the wear volume of the non-reinforced Hovadur® CNCS sample was almost linear. There was only a slight difference in wear volume between the non-reinforced and the

reinforced sample. The second period began at a test time of two hours featuring a linear growth and extended to the end of the experiment at a test time of six hours. The difference between the non-reinforced and the reinforced sample increased with time.

The wear progressions of the Hovadur® CNCS samples are typical for sliding abrasion [27]. The first period is called the run-in period. During this run-in period, the microgeometry changes. Initial peaks in the surface roughness are more and more smoothened which has a decreasing effect on the gradient of the wear volume. The wear progress is described by a square root function. In the second period, the probability of wear processes is constant leading to a constant growth

Warneke 2020   BIAS ID 200707

Fig. 16 Geometrical analysis: run-in behavior of a pin that moved on an FTC particle reinforced Hovadur® CNCS sample. Test force = 30 N, FTC particle content = 40 vol%. The standard deviation is based on six measurements of the wear height
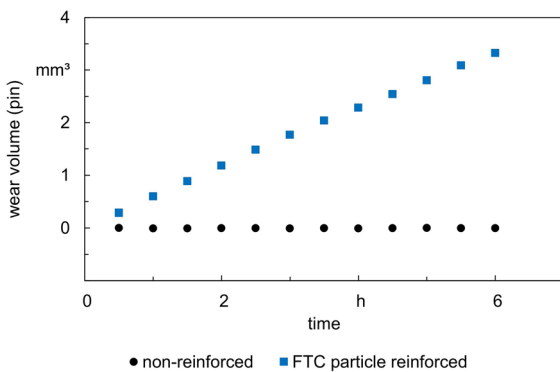
Warneke 2020   BIAS ID 200709

Fig. 17 Gravimetrical analysis: run-in behavior of pins that moved on a non-reinforced and an FTC particle reinforced Hovadur® CNCS sample. Test force = 30 N, FTC particle content = 40 vol%. The standard deviation is based on three weight measurements and is too small for being identifiable in the diagram

of the wear volume. In some cases, a third period may occur that is characterized by an exponential growth of wear. The exponential growth is caused when wear processes accumulate leading to a proportional correlation between wear volume and wear velocity. This third period was not detected in the examined wear-time behavior of the Hovadur® CNCS samples. On the FTC particle reinforced Hovadur® CNCS samples, an exponential growth might occur when FTC particles would break out of the matrix. The break-out of the FTC particles might lead to an increase in wear velocity due to the missing wear protection by the FTC particles. However, within the examined scope of six hours, a third period did not occur.

The wear-time diagrams of the counter bodies are shown in Figs. 16 and 17. No wear was measured on the pin that moved on the non-reinforced Hovadur® CNCS sample. A

geometrical analysis of this pin was not possible. In contrast, strong wear occurred on the pin that moved on the FTC particle reinforced Hovadur® CNCS sample. There was a degressive increase in the wear height and a linear increase in the wear volume of the pin. In contrast to the Hovadur® CNCS samples, only one period was determined for the pins within the scope of the experiment.

4 Conclusions

It was shown that the FTC reinforcement of the copper alloy Hovadur® CNCS, that is used for pistons in pressure die casting, led to a significant improvement in wear resistance against the hardened and gas nitrided steel 1.2343, that is used for shot sleeves in pressure die casting. However, high wear of the hardened and gas nitrided steel 1.2343 was observed when moving against FTC reinforced Hovadur® CNCS. Both on non-reinforced and on FTC particle reinforced Hovadur® CNCS, abrasion and adhesion were the dominant wear mechanisms. However, on FTC particle reinforced Hovadur® CNCS, the FTC particles withstand adhesion. The investigation of the wear volume over time showed that non-reinforced and FTC particle reinforced Hovadur® CNCS featured a similar wear volume progression. After a run-in period, in which the gradient in wear volume decreased, the wear volume grew constantly.

Declarations

References

1. Miklin A (2010) Entwicklung einer Fertigungstechnologie für dünnwandigen Stahlguss. Dissertation, Technische Universität Bergakademie Freiberg

2. Silva F, Campilho RD, Ferreira LP, Pereira MT (2018) Establishing guidelines to improve the high-pressure die casting process of complex aesthetics parts. In: Peruzzini M, Pellicciari M, Bil C, Stjepandić J, Wognum N (eds) Transdisciplinary engineering methods for social innovation of industry 4.0: proceedings of the 25th ISPE Inc. International conference on transdisciplinary engineering, July 3–6, 2018. IOS Press, Amsterdam, Berlin, Washington, DC, pp 887–896. https://doi.org/10.3233/978-1-61499-898-3-887

3. Shabani M, Paydar MH, Zamiri R, Goodarzi M, Moshksar MM (2016) Microstructural and sliding wear behavior of SiC-particle reinforced copper matrix composites fabricated by sintering and sinter-forging processes. J Market Res 5:5–12. https://doi.org/10.1016/j.jmrt.2015.03.002

4. Tjong S, Lau K (2000) Abrasive wear behavior of TiB2 particle-reinforced copper matrix composites. Mater Sci Eng A 282:183–186. https://doi.org/10.1016/S0921-5093(99)00752-2

5. Deshpande PK, Li JH, Lin RY (2006) Infrared processed Cu composites reinforced with WC particles. Mater Sci Eng A 429:58–65. https://doi.org/10.1016/j.msea.2006.04.124

6. Barmouz M, BesharatiGivi MK, Seyfi J (2011) On the role of processing parameters in producing Cu/SiC metal matrix composites via friction stir processing: Investigating microstructure, microhardness, wear and tensile behavior. Mater Charact 62:108–117. https://doi.org/10.1016/j.matchar.2010.11.005

7. Ayers JD, Tucker TR (1980) Particulate-TiC-hardened steel surfaces by laser melt injection. Thin Solid Films 73:201–207. https://doi.org/10.1016/0040-6090(80)90352-1

8. Spranger F, Schirdewahn S, Kromm A, Merklein M, Hilgenberg K (2020) On the influence of TiB2, TiC, and TiN hard particles on the microstructure of localized laser dispersed AISI D2 tool steel surfaces. J Laser Appl 32:22028. https://doi.org/10.2351/7.0000059

9. Student M, Pokhmurska H, Zadorozhna K, Dzyubyk A, Khomych I (2018) Structure and wear resistance of aluminium alloys coated with surface layer laser-modified by silicon carbide. Ukrain J Mech Eng Mater Sci 4:49–57. https://doi.org/10.23939/ujmems2018.01.049

10. Ditsche A, Seefeld T (2020) Local laser particle fusion: fusing of hard particles for the reduction of high contact pressures in MMC tool surfaces. JOM 72:2488–2496. https://doi.org/10.1007/s11837-020-04190-9

11. Vreeling JA, Ocelik V, de Hosson JTM (2002) Ti–6Al–4V strengthened by laser melt injection of WCp particles. Acta Mater. https://doi.org/10.1016/S1359-6454(02)00366-X

12. Günther K, Bergmann JP (2018) Understanding the dissolution mechanism of fused tungsten carbides in Ni -based alloys: an experimental approach. Mater Lett 213:253–256. https://doi.org/10.1016/j.matlet.2017.11.088

13. Nowotny S, Berger L-M, Spatzier J (2014) Coatings by laser cladding. In: Sarin VK, Mari D, Llanes L (eds) Comprehensive hard materials. Elsevier, Amsterdam, pp 507–525. https://doi.org/10.1016/B978-0-08-096527-7.00018-0

14. Pelaprat J-M, Zediker M, Finuf M, Fritz R (2020) The Blue Light District. PhotonicsViews 17:61–65. https://doi.org/10.1002/phvs.202000005

15. Warneke P, Seefeld T (2019) High-speed laser melt injection of tungsten carbide in highly conductive copper alloys. KEM 809:94–99. https://doi.org/10.4028/www.scientific.net/KEM.809.94

16. Deshpande PK, Lin RY (2006) Wear resistance of WC particle reinforced copper matrix composites and the effect of porosity. Mater Sci Eng A 418:137–145. https://doi.org/10.1016/j.msea.2005.11.036

17. Schmelzmetall Deutschland GmbH (2014) Werkstoffdatenblatt Hovadur CNCS. https://www.schmelzmetall.com/fileadmin/downloads/hovadur/hovadur-cncs-de.pdf. Accessed 13 Aug 2020

18. Oerlikon Metco (2016) Material product data sheet—spherical cast tungsten carbide powder for laser cladding. https://www.oerlikon.com/metco/en/products-services/coating-materials/laser-pta-weld-overlay/laser-cladding/. Accessed 13 Aug 2020

19. Stauber GmbH Metalltechnologie Werkstoff 1.2343 Datenblatt. https://www.stauberstahl.com/werkstoffe/12343-werkstoff-datenblatt/. Accessed 14 Aug 2020

20. Brust S (2017) Entwicklung abrasionsbeständiger Metallmatrix-Verbundwerkstoffe auf Eisenbasis mit ionisch-kovalenten Hartstoffen unter Betrachtung der Metall-Keramik-Interaktion. Dissertation, Ruhr Universität Bochum

21. DIN DeutschesInstitutfürNormunge.V. (2010) Hochleistungskeramik - Verfahren zur Prüfung keramischer Schichten - Teil 12: Schwingungs-Verschleißprüfung. Deutsche Fassung EN 1071–12:2010

22. Ala-Kleme S, Kivikytö-Reponen P, Liimatainen J, Hellman J, Hannula S-P (2007) Abrasive wear properties of tool steel matrix composites in rubber wheel abrasion test and laboratory cone crusher experiments. Wear 263:180–187. https://doi.org/10.1016/j.wear.2007.01.111

23. Verma V, Tewari PC, Ahamed RZ, Ahmed ST (2019) Effect of addition of fly ash and Al_2O_3 particles on mechanical and tribological behavior of Al MMC at varying load, time and speed. Procedia Struct Integr 14:68–77. https://doi.org/10.1016/j.prostr.2019.05.010

24. Berns H (2003) Comparison of wear resistant MMC and white cast iron. Wear 254:47–54. https://doi.org/10.1016/S0043-1648(02)00300-9

25. Warneke P, Seefeld T (2020) Wear resistance of hard particle reinforced copper alloys generated by laser melt injection. DDF 404:68–76. https://doi.org/10.4028/www.scientific.net/DDF.404.68

26. Freiße H, Ditsche A, Seefeld T (2019) Reducing adhesive wear in dry deep drawing of high-alloy steels by using MMC tool. Manuf Rev 6:12. https://doi.org/10.1051/mfreview/2019004

27. Czichos H (2015) Tribologie Handbuch, 4th edn. Springer, Wiesbaden